J|A|C|S COMMUNICATIONS

Published on Web 12/09/2009

One-Pot Nucleation, Growth, Morphogenesis, and Passivation of 1.4 nm Au Nanoparticles on Self-Assembled Rosette Nanotubes

Rahul Chhabra,[†,‡] Jesus G. Moralez,[†,‡] Jose Raez,[†,‡] Takeshi Yamazaki,[†,§] Jae-Young Cho,[†] Andrew J. Myles,[†] Andriy Kovalenko,[†,§] and Hicham Fenniri*[,†,‡]

National Institute for Nanotechnology (NINT-NRC), Department of Chemistry, and Department of Mechanical Engineering, University of Alberta, 11421 Saskatchewan Drive, Edmonton, Alberta, Canada T6G 2M9

Received October 21, 2009; E-mail: hicham.fenniri@nrc-cnrc.gc.ca

The modification of biomolecules with metal-based nanoparticles (NPs) allows us to create materials with exciting new properties for applications in medicine, molecular electronics, optics, and catalysis.[1] Researchers have been able to perform electroless deposition of NPs on DNA,[2] peptide complexes,[3] polymers,[4] and nanotubes such as the tobacco mosaic virus,[5] peptide nanotubes,[6] and DNA-based nanotubes.[7] However, coverage of the organic structure generally has been incomplete and the NP size distribution relatively broad. Sequence-specific deposition of Ag and Au NPs on DNA was previously achieved on fully stretched DNA molecules on silicon substrates.[8] In this case, nucleoprotein strands composed of RecA proteins bound to a sequence-specific DNA strand acted as a negative resist and protected specific regions of DNA from metallization. This approach was indeed a great advancement in the control of selective metallization of DNA, but this type of control has not been achieved to date in synthetic self-assembled nanostructures. Here we report a one-pot process for the site-specific nucleation, growth, morphogenesis, and passivation of 1.4 nm Au NPs on self-assembled rosette nanotubes (RNTs).

RNTs are a new class of biocompatible materials obtained through self-assembly of a synthetic DNA base analogue, the G∧C motif. Intermolecular hydrogen bonding mediates the self-assembly of six heteroaromatic G∧C bases in water to form a supermacrocycle (rosette) maintained by 18 H bonds. The resulting and substantially more hydrophobic rosettes then self-organize to produce a tubular stack with tunable dimensions and properties.[9] The RNTs used in this study were assembled from a heteroaromatic bicyclic twin G∧C base (**1**, Figure 1A), which upon self-assembly forms a twin rosette maintained by 36 H bonds (Figure 1B) and then a helical stack (Figure 1C).[9d]

To assemble the RNTs, **1** was dissolved in water (1 mM), heated for 20 min at 90 °C in an oil bath, and aged at room temperature for 24 h to ensure complete self-assembly. This solution was then diluted to 50 μM, and a sample (5 μL) was deposited on freshly cleaved mica and imaged by tapping-mode atomic force microscopy (TM-AFM) and scanning electron microscopy (SEM) (Figure 2). The AFM height profile of the RNTs was ∼3 nm, which is significantly lower than the measured (4.0 ± 0.3 nm) and calculated (4.0 nm) outer diameter. As in earlier reports, this discrepancy was attributed to the compressibility of the RNTs under the AFM tip.[9d] Both TM-AFM and SEM images confirmed the formation of RNTs with lengths of several micrometers.

To incorporate Au NPs on the self-assembled RNTs, we reasoned that the positively charged lysine side chains would coordinate to the negatively charged tetrachloroaurate ($AuCl_4^-$). Upon reduction with hydrazine (N_2H_4), each lysine site could then act as a nucleation point for the formation of Au NPs. Thus, the [**1**]/[$HAuCl_4$] ratio was optimized to maximize the loading of Au NPs on the surface of the RNTs. We found that a 1:20 [**1**]/[$HAuCl_4$] molar ratio gave the desired outcome. Below this ratio, the loading was insufficient, and a higher ratio resulted in polydisperse Au aggregates (data not shown). For the same reason, we established experimentally that the [$HAuCl_4$]/

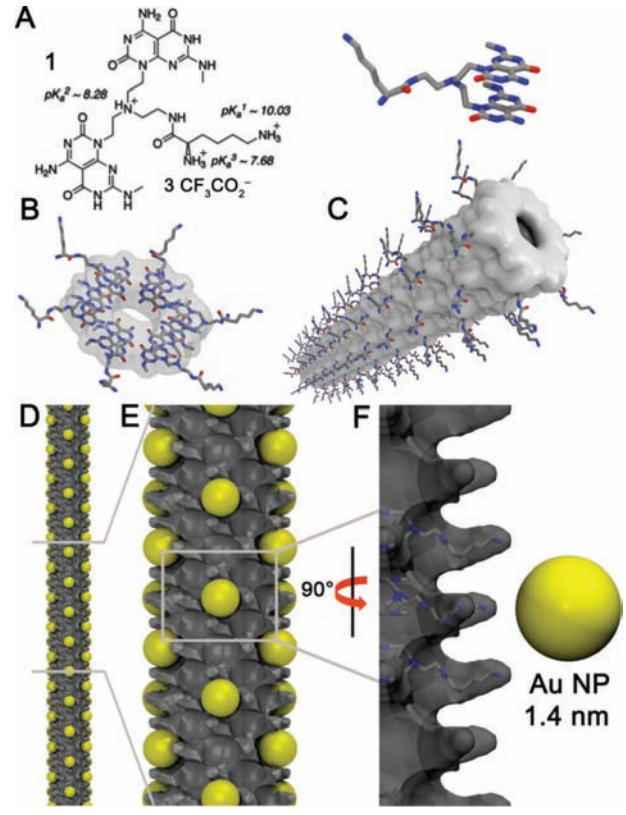

Figure 1. Schematic of the RNTs as nucleation templates. (A) Twin G∧C base **1**. (B) Self-assembled rosette. (C) Self-assembled RNT obtained from rosette stacking. (D, E) RNTs with nucleated Au NPs (gold spheres). (F) Close-up view of the nucleation site.

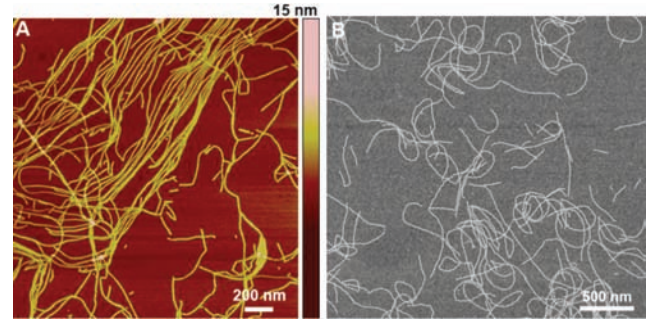

Figure 2. (A) TM-AFM image of RNTs on mica and (B) SEM micrograph of the same sample on a carbon-coated copper grid.

[†] National Institute for Nanotechnology.
[‡] Department of Chemistry.
[§] Department of Mechanical Engineering.

10.1021/ja908775g

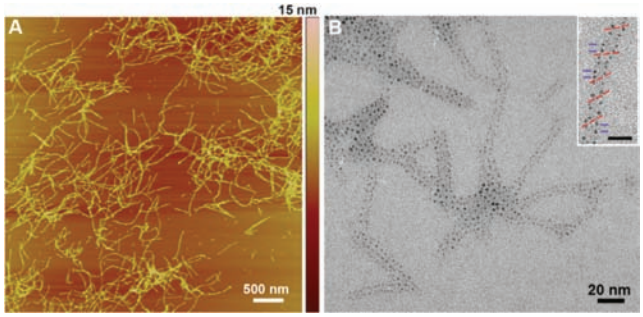

Figure 3. (A) TM-AFM image of Au NP-coated RNTs on mica. (B) TEM image showing monodisperse Au NP/RNT composite on a carbon-coated grid. The inset shows a helical organization of Au NPs on RNT templates; the red lines indicate the pitch angle, and the blue lines indicate the distance between adjacent Au NPs (scale bar = 10 nm).

$[N_2H_4 \cdot H_2O]$ molar ratio had to be kept constant (10:1) to ensure a narrow size distribution of Au NPs on the RNT templates.

In a typical experiment, a solution of **1** in water (200 μL, 50 μM, pH 5−6) was mixed with $HAuCl_4$ (2 μL, 0.1 M) and incubated in the dark for 24 h (final pH ∼3). $N_2H_4 \cdot H_2O$ (2 μL, 0.01 M) was then added to the reaction mixture (final pH ∼3). It was important to have excess $AuCl_4^-$ ions, as these ions contribute to the colloidal stability of the newly formed Au NPs.[10] A statistical analysis of the particle diameter and interparticle distance by transmission electron microscopy (TEM) was carried out on several hundred Au NPs and revealed a mean diameter of 1.4 ± 0.2 nm and a mean interparticle distance of 3.8 ± 0.8 nm.

In an attempt to increase the Au NP loading on the RNTs, the concentration of **1** was increased from 50 μM to 1 mM while maintaining the same [**1**]/[$HAuCl_4$] and [$HAuCl_4$]/[$N_2H_4 \cdot H_2O$] ratios. Addition of $HAuCl_4$ resulted in a pH decrease from 3.5 to 1.7, and the pH remained constant after addition of $N_2H_4 \cdot H_2O$. In this case, the mean NP diameter was found to be 1.5 ± 0.1 nm with an interparticle distance of 3.5 ± 0.4 nm. The similarity of the Au NPs sizes was attributed to the templating effect of the RNTs (see below). TM-AFM images of this sample showed the formation of rigid threadlike structures with a height of ∼4.6 nm (Figure 3A), in excellent agreement with the calculated diameter of the Au NP/RNT composite (Figure S8 in the Supporting Information). TEM analysis unambiguously established the RNTs' ability to nucleate and template the growth and morphogenesis of the Au NPs, which appear as small dots on the RNT surface (Figure 3B). Their size distribution is remarkably narrow relative to that in previously reported systems.[11] Furthermore, the size of 1.4−1.5 nm suggests that these NPs are likely Schmid's clusters (Au_{55}).[12] To further confirm this hypothesis, energy-dispersive X-ray (EDX) analysis and selected-area electron diffraction were carried out (Figures S2 and S3).

Analysis of the organization of the Au NPs in several TEM images revealed a helical arrangement on the RNTs with a pitch angle of 40.1 ± 2.3° (Figure 3B inset and Figure S8); the shortest distance between Au NPs along the long axis of the RNT was 3.5 ± 0.3 nm (the distance between blue lines in the Figure 3B inset), and that across the RNT was 4.2 ± 0.3 (the wall-to-wall distance). On the basis of these observations, the model in Figure 1D−F was built. This model shows pockets with a cross section of 1.6 nm defined by four adjacent lysine side chains (Figure 1F) that can accommodate a 1.4−1.5 nm Au NP. The next available pocket along the main axis of the RNT is 1.4−1.6 nm away, thus resulting in an interparticle distance of ∼3.2 nm (Figure S8). However, at a ±20° angle on each side of each pocket, additional nucelation sites are available, accounting for the angular relationship between Au NPs.

A statistical analysis of the TEM images revealed that out of the maximum number of sites (188 sites/100 nm), only ∼30% were filled (58 sites/100 nm). Figure S8A,B shows two models: (A) a theoretical maximum occupancy model and (B) a zigzag model based on the TEM measurements. The zigzag model not only accounts for the ∼30% loading and interparticle distances measured but also indicates reduced interparticle repulsion, as each nucleation site is surrounded with four unoccupied sites. The open versions of the maximum occupancy and zigzag models are shown in Figure S8C,D.

Since the majority of the Au NPs are located on the RNTs, we believe that the low loading is due to either (a) electrostatic repulsion between Au NPs or (b) incomplete loading due to limited supply of reducing agent (the limiting reagent in this system). To test the second hypothesis, we added excess hydrazine (10 and 100 equiv relative to **1**), but this resulted in the formation of large polydisperse particles without improving the RNT loading. Therefore, we believe that the maximum loading of this particular RNT cannot exceed ∼30%, most likely for electrostatic reasons.

Each nucleation pocket is composed of four adjacent lysine side chains wherein each lysine could accommodate three $AuCl_4^-$ ions, correlating with the protonation states of the lysine side chain (Figure 1A). Thus, on the basis of the zigzag model (∼30% occupancy with Au_{55} NPs) each equivalent of molecule **1** would require ∼4.1 equiv of Au(III) and 6.2 equiv of N_2H_4 [i.e., 3 molar equiv of N_2H_4 for every 2 mol equiv of Au(III)]. Experimentally, we used 20 equiv of Au(III) (i.e., ∼5 fold excess for the zigzag model) but only 2 equiv of N_2H_4 relative to compound **1** (i.e., ∼3 fold less than what is needed for the conversion of all of the RNTs to the zigzag model). On the basis of this estimate, one should expect the distribution of Au NPs on the RNTs to be less dense, which leads us to speculate that a significant proportion of RNTs that aggregate in the presence of excess $AuCl_4^-$ ions were not exposed to N_2H_4.

In conclusion, we have demonstrated that self-assembled RNTs can be used to nuclate nearly monodisperse Au NPs. Future studies include the nucleation of other metal NPs for applications in catalysis, nanoelectronics, and nanophotonics.

Acknowledgment. We thank NIH (NIH EB03824), NSERC, NRC, and the University of Alberta for supporting this program. J.G.M. thanks NIH (GM55146-08) for a graduate fellowship.

Supporting Information Available: Experimental details and additional figures. This material is available free of charge via the Internet at http://pubs.acs.org.

References

(1) (a) Daniel, M.-C.; Astruc, D. *Chem. Rev.* **2004**, *104*, 293. (b) Rosi, N. L.; Mirkin, C. A. *Chem. Rev.* **2005**, *105*, 1547.
(2) Yan, H.; Park, S. H.; Finkelstein, G.; Reif, J. H.; LaBean, T. H. *Science* **2003**, *301*, 1882.
(3) Chen, C.-L.; Zhang, P.; Rosi, N. L. *J. Am. Chem. Soc.* **2008**, *130*, 13555.
(4) Ofir, Y.; Samanta, B.; Rotello, V. M. *Chem. Soc. Rev.* **2008**, *37*, 1814.
(5) Knez, M.; Bittner, A. M.; Boes, F.; Wege, C.; Jeske, H.; Maiss, E.; Kern, K. *Nano Lett.* **2003**, *3*, 1079.
(6) Carny, O.; Shalev, D. E.; Gazit, E. *Nano Lett.* **2006**, *6*, 1594.
(7) (a) Liu, D.; Park, S. H.; Reif, J. H.; LaBean, T. H. *Proc. Natl. Acad. Sci. U.S.A.* **2004**, *101*, 717. (b) Sharma, J.; Chhabra, R.; Cheng, A.; Brownell, J.; Liu, Y.; Yan, H. *Science* **2009**, *323*, 112.
(8) Keren, K.; Krueger, M.; Gilad, R.; Ben-Yoseph, G.; Sivan, U.; Braun, E. *Science* **2002**, *297*, 72.
(9) (a) Fenniri, H.; Mathivanan, P.; Vidale, K. L.; Sherman, D. M.; Hallenga, K.; Wood, K. V.; Stowell, J. G. *J. Am. Chem. Soc.* **2001**, *123*, 3854. (b) Fenniri, H.; Deng, B.-L.; Ribbe, A. E. *J. Am. Chem. Soc.* **2002**, *124*, 11064. (c) Chun, A.; Moralez, J. G.; Fenniri, H.; Webster, T. J. *Nanotechnology* **2004**, *15*, S234. (d) Moralez, J. G.; Raez, J.; Yamazaki, T.; Motkuri, R. K.; Kovalenko, A.; Fenniri, H. *J. Am. Chem. Soc.* **2005**, *127*, 8307.
(10) Pei, L.; Mori, K.; Adachi, M. *Langmuir* **2004**, *20*, 7837.
(11) Djalali, R.; Chen, Y.; Matsui, H. *J. Am. Chem. Soc.* **2002**, *124*, 13660.
(12) Schmid, G. *Chem. Rev.* **1992**, *92*, 1709.

JA908775G